Electronic Supplementary Information (ESI)

New Structure Family of Oxide-ion Conductors Based on $BaGdInO_4$

Hiroshi Yaguchi,[1] Kotaro Fujii,[1] Masatomo Yashima[1,*]

[1] Department of Chemistry, School of Science, Tokyo Institute of Technology, 2-12-1-W4-17, O-okayama, Meguro-ku, Tokyo 152-8551, Japan

Crystal structure of $BaGdInO_4$, $BaNdInO_4$ and $SrYbInO_4$

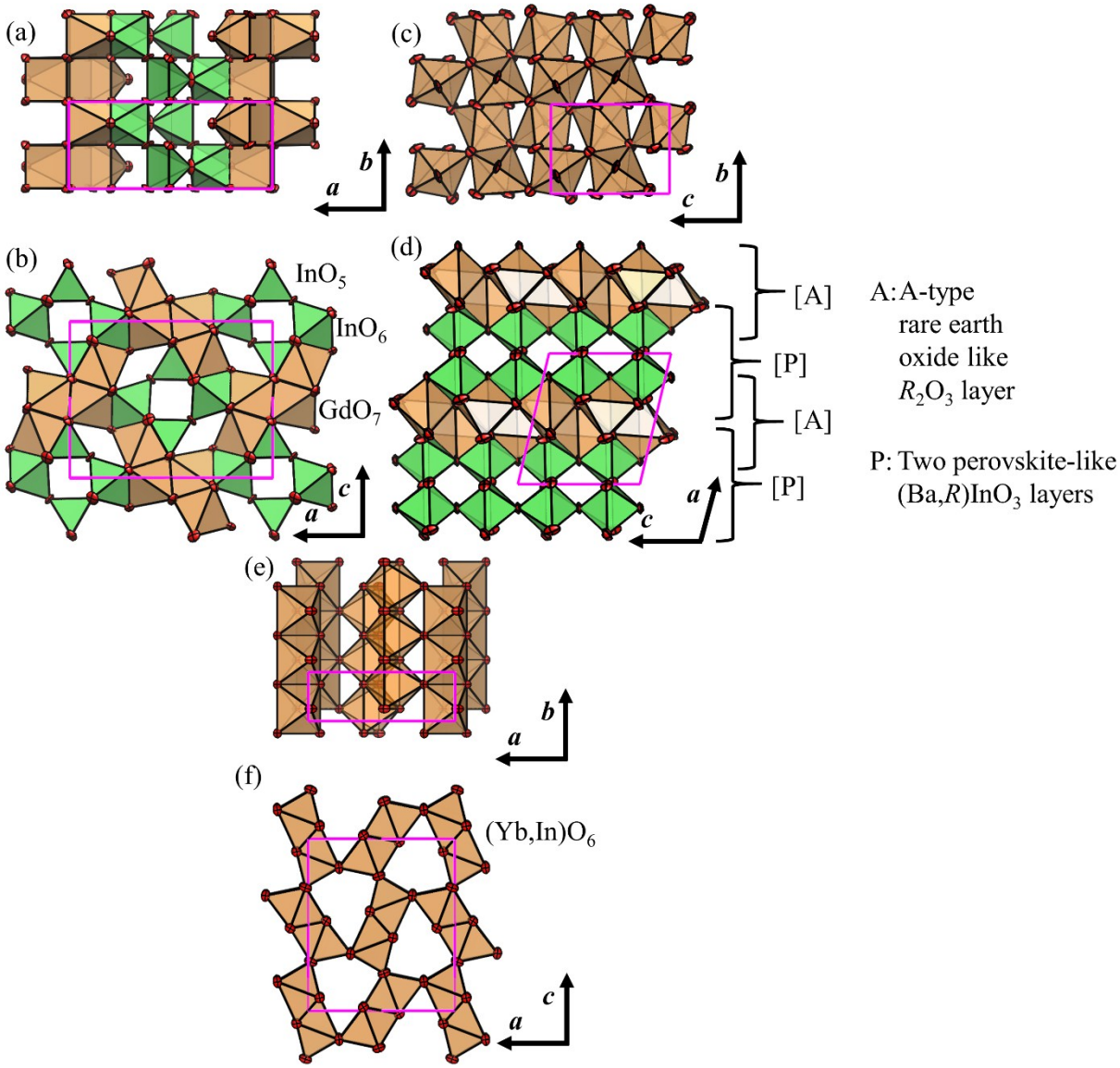

Fig. S1 Crystal structure of $BaGdInO_4$ viewed (a) along the *c* axis ($-0.1 \le x \le 1.1$; $0.0 \le y \le 2.0$; $0.25 \le z \le 0.75$) and (b) along the *b* axis ($-0.2 \le x \le 1.2$; $0.0 \le y \le 1.0$; $-0.25 \le z \le 1.25$). Red ellipsoids, green and orange polyhedra stand for oxygen atoms, InO_n (n = 5 and 6) and GdO_7, respectively. Crystal structure of $BaNdInO_4$ (= $BaRInO_4$; R = Nd) viewed (c) along the *a* axis ($0.3 \le x \le 0.6$; $0.0 \le y \le 2.0$; $0.0 \le z \le 2.0$) and (d) along the *b* axis ($-0.2 \le x \le 1.6$; $0.0 \le y \le 1.0$; $0.0 \le z \le 2.0$). Red ellipsoids, green and orange polyhedra stand for oxygen atoms, InO_6 octahedron and NdO_7 polyhedron, respectively. Crystal structure of $SrYbInO_4$ (e) along the *c* axis ($-0.2 \le x \le 1.2$; $0.0 \le y \le 3.2$; $-0.2 \le z \le 0.2$) and (f) along the *b* axis ($-0.2 \le x \le 1.2$; $0.0 \le y \le 1.0$; $-0.2 \le z \le 1.2$). Red ellipsoids and orange polyhedron stand for oxygen atoms and $(Yb,In)O_6$ octahedron, respectively. Thermal ellipsoids are drawn at the 99% probability level. Pink solid lines denote the unit cells. Ba and Sr atoms are omitted in panels a-d and e,f, respectively, for simplicity.

Crystal structure analysis of SCXRD data of $BaGdInO_4$

In preliminary analyses of SCXRD data of $BaGdInO_4$, the occupancy factors of *X* atom at the *s* site *g*(*X*; *s*) were refined as follows. *g*(Ba; Ba1) = 0.998(10), *g*(Ba; Ba2) = 1.000(10), *g*(Gd; Gd1) = 0.991(10), *g*(Gd; Gd2) = 0.988(10), *g*(In; In1) = 1.005(10), *g*(In; In2) = 0.997(10), *g*(O; O1) = 1.045(18), *g*(O; O2) = 1.039(18), *g*(O; O3) = 1.031(14), *g*(O; O4) = 1.030(14), *g*(O; O5) = 1.015(15). All the occupancy factors agreed to unity within three times of estimated standard deviations. Therefore, all the occupancy factors were fixed to unity in the final refinement. Results of the final structure refinement of the SCXRD data of $BaGdInO_4$ are listed in Tables 1 and S1.

Table S1 Refined anisotropic atomic displacement parameters of $BaGdInO_4$ obtained by structure analyses of SCXRD data.

Site label	U_{11} (Å^2)	U_{22} (Å^2)	U_{33} (Å^2)	U_{12} (Å^2)	U_{13} (Å^2)	U_{23} (Å^2)
Ba1	0.00785(12)	0.00722(13)	0.00831(13)	0	0.00127(10)	0
Ba2	0.01390(14)	0.00892(14)	0.00903(14)	0	0.00086(12)	0
Gd1	0.00498(10)	0.00433(10)	0.00510(10)	0	0.00060(8)	0
Gd2	0.00626(10)	0.00456(10)	0.00480(10)	0	0.00003(8)	0
In1	0.00373(13)	0.00382(13)	0.00389(14)	0	−0.00031(11)	0
In2	0.00441(13)	0.00348(14)	0.00460(15)	0	0.00045(11)	0
O1	0.0084(16)	0.0110(18)	0.0059(16)	0	0.0013(14)	0
O2	0.0067(16)	0.024(2)	0.0083(18)	0	−0.0049(14)	0
O3	0.0091(12)	0.0089(13)	0.0118(13)	0.0032(10)	−0.0026(11)	0.0005(9)
O4	0.0102(12)	0.0088(13)	0.0103(13)	0.0035(10)	0.0025(10)	−0.0014(10)
O5	0.0140(13)	0.0075(12)	0.0136(14)	−0.0015(10)	0.0028(12)	0.0062(10)

Rietveld analysis of synchrotron X-ray powder diffraction data of $BaGdInO_4$ and $BaGd_{0.9}Ca_{0.1}InO_{3.95}$

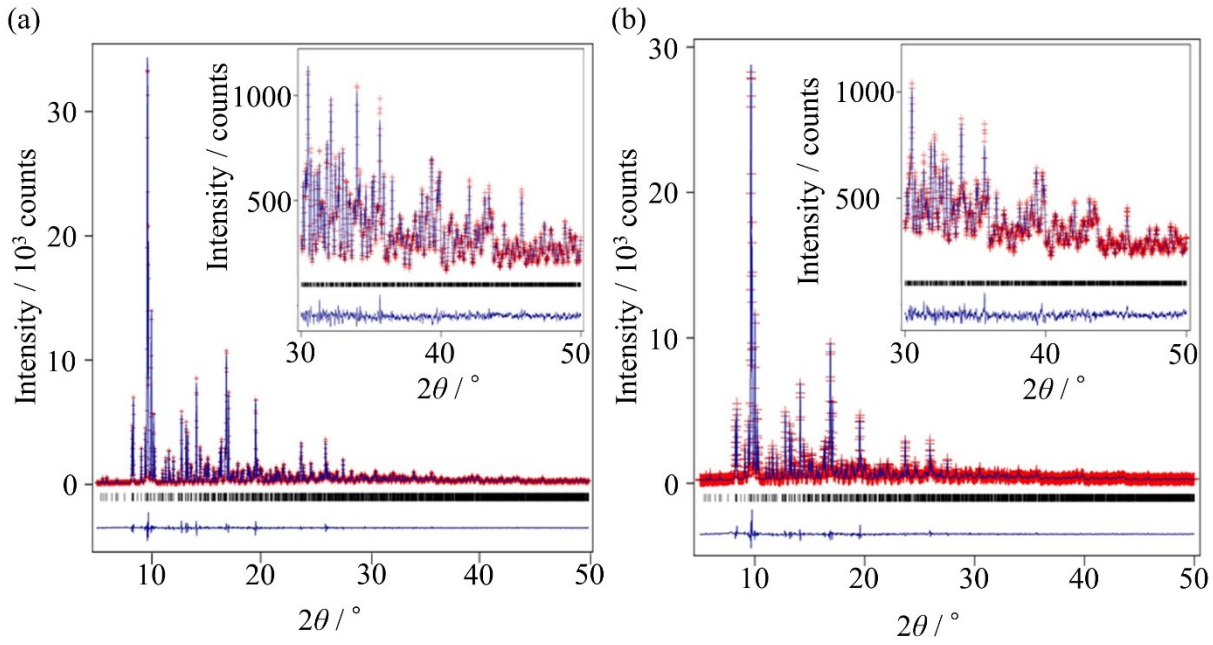

Fig. S2 Rietveld patterns for synchrotron X-ray powder diffraction (SXRPD) data of (a) $BaGdInO_4$ and (b) $BaGd_{0.9}Ca_{0.1}InO_{3.95}$, showing the experimental data (red + marks), calculated intensities (blue solid line) and difference pattern (blue solid line). Black tick marks in panels (a) and (b) denote calculated Bragg peak positions of orthorhombic $BaGdInO_4$ and $BaGd_{0.9}Ca_{0.1}InO_{3.95}$, respectively.

Table. S2 Crystallographic data of $BaGdInO_4$ and $BaGd_{0.9}Ca_{0.1}InO_{3.95}$.[a]

Chemical formula	$BaGdInO_4$	$BaGd_{0.9}Ca_{0.1}InO_{3.95}$
Formula weight	946.82	923.39
Temperature / °C	20	20
Wavelength / Å	0.4994152(11) Å	
Crystal system	Orthorhombic	
Space group	*Pnma*	
a / Å	13.78294(6)	13.79264(9)
b / Å	5.88350(3)	5.87779(4)
c / Å	10.62552(5)	10.62782(7)
V / Å	861.644(12)	861.600 (16)
R_{wp}*	0.060	0.059
R_B*	0.023	0.031
R_F*	0.013	0.015

[a]Crystallographic data of $BaGdInO_4$ and $BaGd_{0.9}Ca_{0.1}InO_{3.95}$ were obtained by the Rietveld analyses of the synchrotron X-ray powder diffraction data taken by the Debye-Scherrer camera with the imaging plate installed at the BL-19B2 beam line of SPring-8.

*R_{wp} is the weighted profile reliability factor, and R_B and R_F are the reliability factors based on Bragg intensity and structure factor, respectively.

Table S3 Refined crystallographic parameters and reliability factors in Rietveld analysis of synchrotron X-ray diffraction data of $BaGdInO_4$ measured at 26.7 °C.

Site label	*x*	*y*	*z*	U_{iso} (Å^2)*
Ba1	0. 21432(7)	0.25	0.66662 (9)	0.0057(2)
Ba2	0.09056(7)	0.75	0.89080 (8)	0.0091(2)
Gd1	0.08287(5)	0.75	0.51837 (6)	0.0038(2)
Gd2	0.14334(5)	0.25	0.31182 (6)	0.0038(2)
In1	0.30726(8)	0.75	0.52165 (9)	0.0028(2)
In2	0.02962(8)	0.75	0.22013 (9)	0.0041(2)
O1	0.2060(6)	0.75	0.6863 (8)	0.0102(8)
O2	−0.0987(7)	0.75	0.1334 (7)	= U_{iso}(O1)
O3	0.2099(4)	−0.0027(10)	0.4464 (5)	= U_{iso}(O1)
O4	0.0096(4)	0.4973(12)	0.3651 (5)	= U_{iso}(O1)
O5	0.1132(5)	0.4942(12)	0.1303 (5)	= U_{iso}(O1)

*U_{iso}: Isotropic atomic displacement parameter.

Table S4 Refined crystallographic parameters and reliability factors in Rietveld analysis of synchrotron X-ray diffraction data of $BaGd_{0.9}Ca_{0.1}InO_{3.95}$ measured at 26.7 °C.

Site label *X*	atom *Y*	*g*(*Y*; *X*)*	*x*	*y*	*z*	U_{iso} (Å^2) ****
Ba1	Ba	1	0.21421(9)	0.25	0.66733(11)	0.0089(3)
Ba2	Ba	1	0.09054(10)	0.75	0.89107(11)	0.0131(3)
Gd,Ca1	Gd	0.9	0.08230(8)	0.75	0.51807(8)	0.0033(2)
	Ca	0.1				
Gd,Ca2	Gd	0.9	0.14267(7)	0.25	0.31157(9)	0.0024(2)
	Ca	0.1				
In1	In	1	0.30659(10)	0.75	0.52145(12)	0.0045(3)
In2	In	1	0.02973(10)	0.75	0.22054(12)	0.0057(3)
O1	O	0.9875	0.2075(8)	0.75	0.6867(10)	0.0113(10)
O2	O	0.9875	−0.0974(9)	0.75	0.1331(8)	= U_{iso}(O1)
O3	O	0.9875	0.2081(5)	0.0014(12)	0.4478(6)	= U_{iso}(O1)
O4	O	0.9875	0.0123(5)	0.4915(16)	0.3682(6)	= U_{iso}(O1)
O5	O	0.9875	0.1128(6)	0.4909(16)	0.1357(6)	= U_{iso}(O1)

*Occupancy factor of atom *Y* at the *X* site, **U_{iso}: Isotropic atomic displacement parameter.

DFT structure optimization of $BaGdInO_4$

Table S5 Crystal symmetry, space group, lattice and positional parameters of the optimized structure of $BaGdInO_4$ obtained by DFT calculations and difference between the parameters optimized by DFT calculation and those refined by the SCXRD analyses (Table 1).

Crystal symmetry: orthorhombic, Space group: *Pnma*

(a) Optimized lattice parameters

	Optimized lattice parameter	Difference / %
a / Å	13.958	1.01
b / Å	5.927	1.01
c / Å	10.728	1.01

(b) Optimized atomic coordinates

	Atomic coordinates			Difference / %		
Site label	*x*	*y*	*z*	*Δx*	*Δy*	*Δ z*
Ba1	0.2168	0.25	0.6651	−0.21	0	0.18
Ba2	0.9083	0.25	0.3128	0.13	0	0.78
Gd1	0.9179	0.25	0.4834	−0.07	0	−0.15
Gd2	0.1423	0.25	0.3128	0.11	0	−0.10
In1	0.6945	0.25	0.4776	−0.17	0	0.04
In2	0.9709	0.25	0.7792	−0.07	0	0.08
O1	0.7943	0.25	0.309	−0.06	0	0.21
O2	0.1032	0.25	0.8645	−0.24	0	0.25
O3	0.2067	0.9987	0.4466	0.25	0.38	−0.15
O4	0.0095	0.5002	0.3664	−0.15	0.35	−0.18
O5	0.112	0.4974	0.1305	−0.04	0.19	−0.19

Lattice parameters *a, b, c* and lattice volume of $BaGd_{0.9}A_{0.1}InO_{3.95}$ (*A* = Mg, Ca, and Sr)

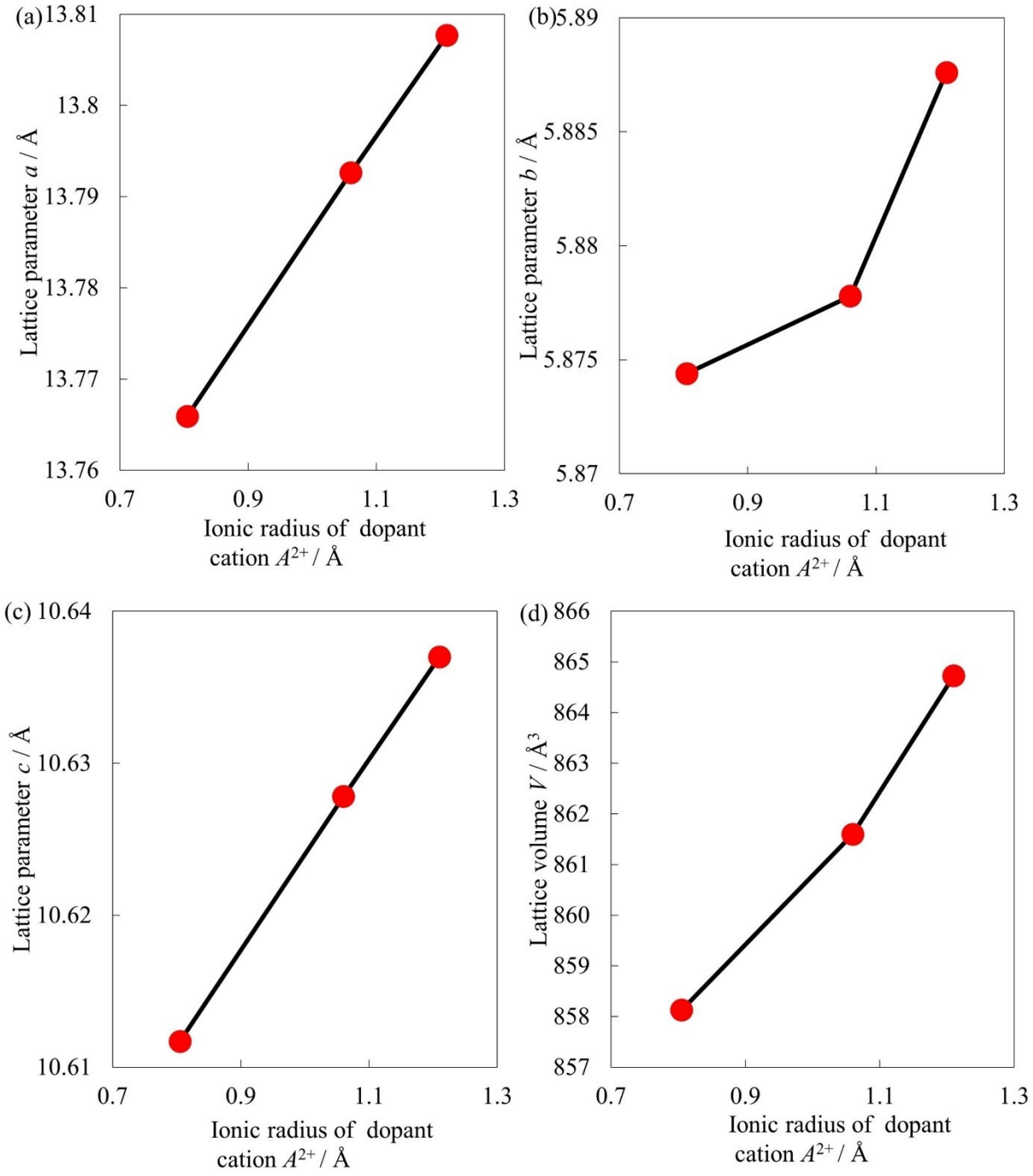

Fig. S3 Lattice parameters (a) *a*, (b) *b*, (c) *c* and (d) lattice volume *V* of $BaGd_{0.9}A_{0.1}InO_{3.95}$ (*A* = Mg, Ca, Sr) as a function of ionic radius of A^{2+} cation. Here, the ionic radii of A^{2+} for the coordination number of seven after Shannon[1] were used.

Electrical, thermal and optical properties of $BaGd_{0.9}Ca_{0.1}InO_{3.95}$ and $BaGdInO_4$

Memo to explain the oxygen partial pressure dependence of total electrical conductivities in Fig. 5.

Total electrical conductivities σ_{total} decreased with decreasing oxygen partial pressure $P(O_2)$ from 0.2 to 4.9×10^{-4} atm (regions [A] in Fig. 5) for $BaGdInO_4$ and from 0.2 to 3.7×10^{-3} atm (region [D] in Fig. 5) for $BaGd_{0.9}Ca_{0.1}InO_{3.95}$. The slopes of $\log(\sigma_{total})$ versus $\log(P(O_2))$ of $BaGdInO_4$ and $BaGd_{0.9}Ca_{0.1}InO_{3.95}$ in the regions [A] and [D] were 0.15(1) and 0.28(3), respectively, which suggests p-type conduction. σ_{total} of $BaGdInO_4$ increased with decreasing $P(O_2)$ from 1.5×10^{-20} to 1.3×10^{-23} atm (region [C] in Fig. 5). The slope of region [C] was 0.228(6), which suggests n-type conduction in the region [C].

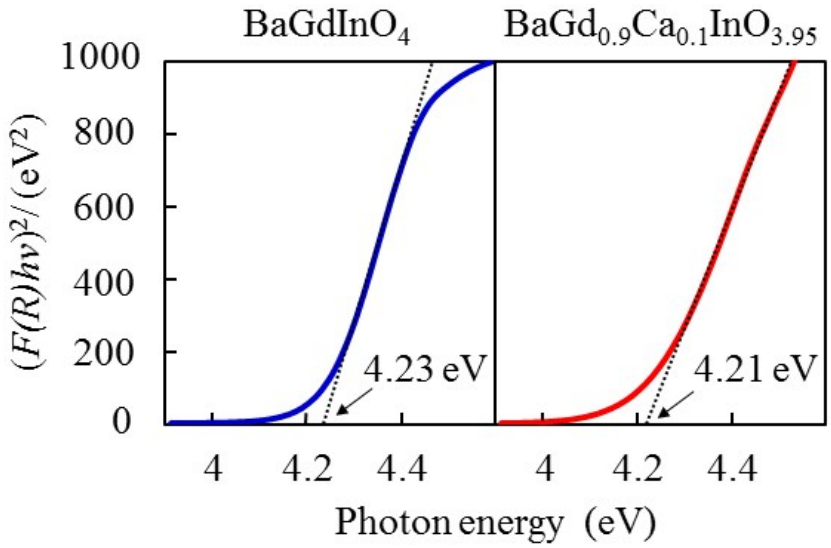

Fig. S4 Tauc plots for the direct band gap of $BaGdInO_4$ (blue solid line) and $BaGd_{0.9}Ca_{0.1}InO_{3.95}$ (red solid line). The band structure obtained by the DFT calculations of $BaGdInO_4$ (Fig. S5) suggested that direct band gap.

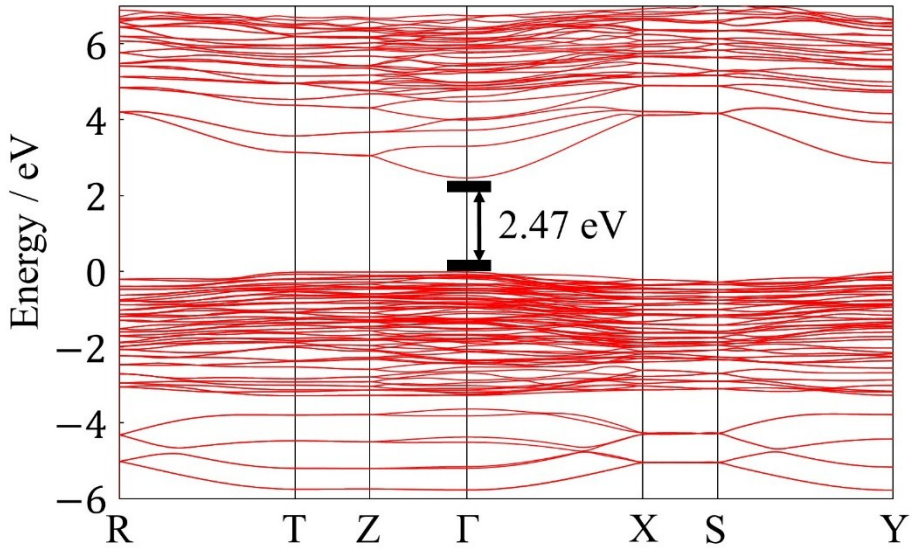

Fig. S5 Band structure of $BaGdInO_4$ based on DFT calculations, which indicates the direct band gap of 2.47 eV.

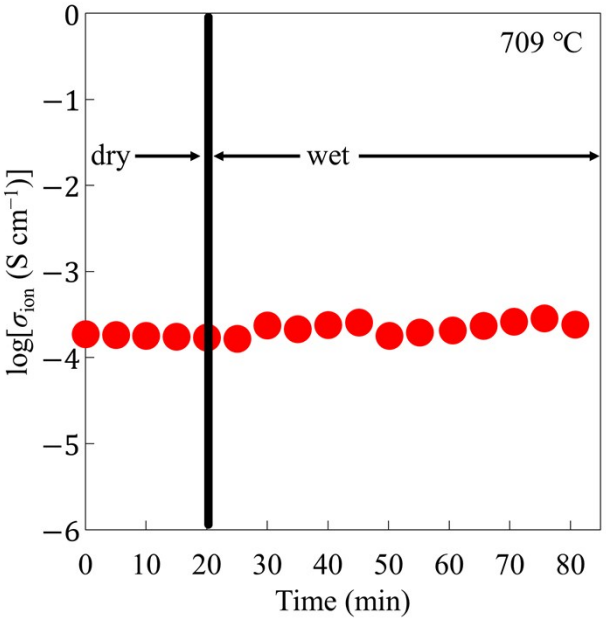

Fig. S6 Oxide-ion conductivity σ_{ion} of $BaGd_{0.9}Ca_{0.1}InO_{3.95}$ in dry and wet ($P(H_2O)$ =2.3×10^{-2} atm) N_2 at 709 °C. σ_{ion} was measured at $P(O_2)$ =1.69×10^{-4} ~ 2.70×10^{-4} atm for $BaGd_{0.9}Ca_{0.1}InO_{3.95}$. The σ_{ion} in Fig. S6 was not corrected using the Bruggeman approximation.

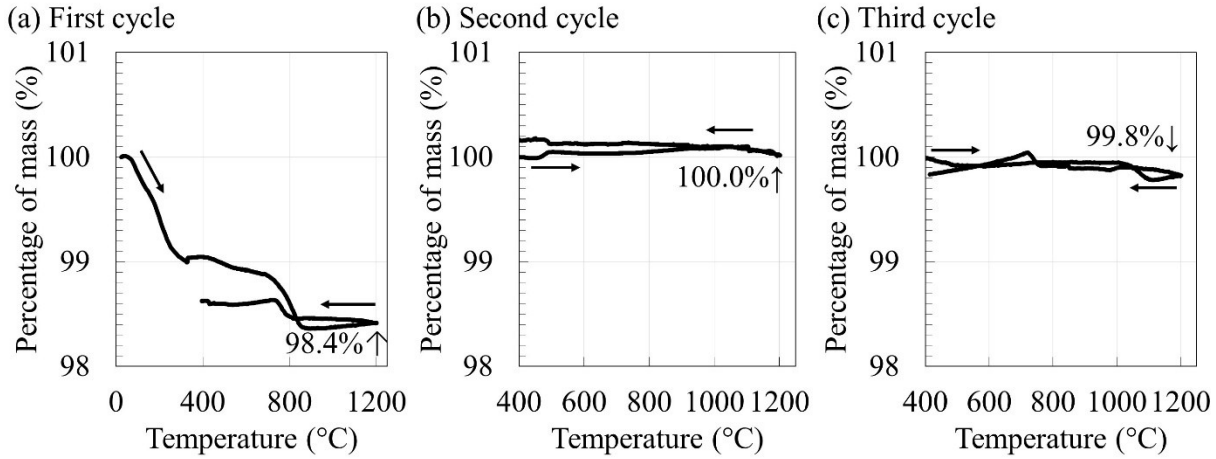

Fig. S7 Results of the thermogravimetric (TG) analysis of $BaGdInO_4$ in (a) first, (b) second and (c) third heating and cooling cycles. TG data in the first cycle for $BaGdInO_4$ showed 1.6 wt% weight loss, which was mainly attributable to the desorption of absorbed species such as water.

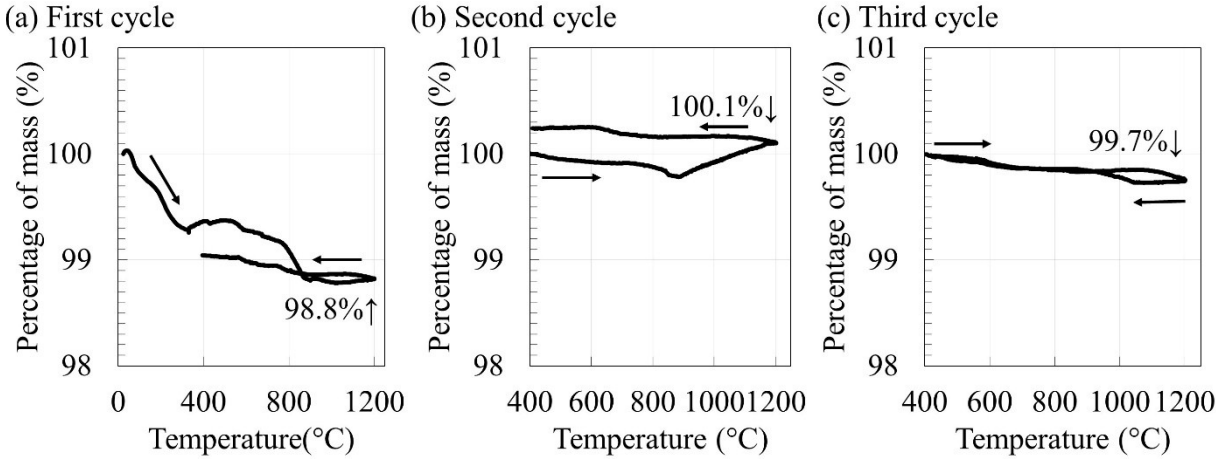

Fig. S8 Results of the thermogravimetric (TG) analysis of $BaGd_{0.9}Ca_{0.1}InO_{3.95}$ in (a) first, (b) second and (c) third heating and cooling cycles. TG data in the first cycle for $BaGd_{0.9}Ca_{0.1}InO_{3.95}$ showed 1.2 wt% weight loss, which was mainly attributable to the desorption of absorbed species such as water.

AC impedance spectra of $BaGd_{0.9}Ca_{0.1}InO_{3.95}$

The electrical conductivities of $BaGd_{0.9}Ca_{0.1}InO_{3.95}$ were measured from 400 to 700 °C by AC impedance spectroscopy. Fig. S9 shows the impedance spectra of $BaGd_{0.9}Ca_{0.1}InO_{3.95}$. The equivalent circuit used to model the impedance data is shown in Fig. S11. The equivalent circuit analyses gave the capacitance values of $C_b = 9 \times 10^{-12}$ F cm^{-1} and $C_{gb} = 1 \times 10^{-10}$ F cm^{-1} in the whole temperature range (Fig. S9). Here the subscripts b and gb denote the bulk and grain boundary, respectively. Fig. S10 shows the temperature dependence of the bulk conductivity σ_b and grain-boundary conductivity σ_{gb} of $BaGd_{0.9}Ca_{0.1}InO_{3.95}$ on cooling. The σ_b and σ_{gb} of $BaGd_{0.9}Ca_{0.1}InO_{3.95}$ increased with an increase in temperature. The σ_b of $BaGd_{0.9}Ca_{0.1}InO_{3.95}$ was higher than that of the ion conductivity (σ_{ion}) by DC 4-probe method. The σ_{ion} of $BaGd_{0.9}Ca_{0.1}InO_{3.95}$ was higher than that of the σ_{gb}.

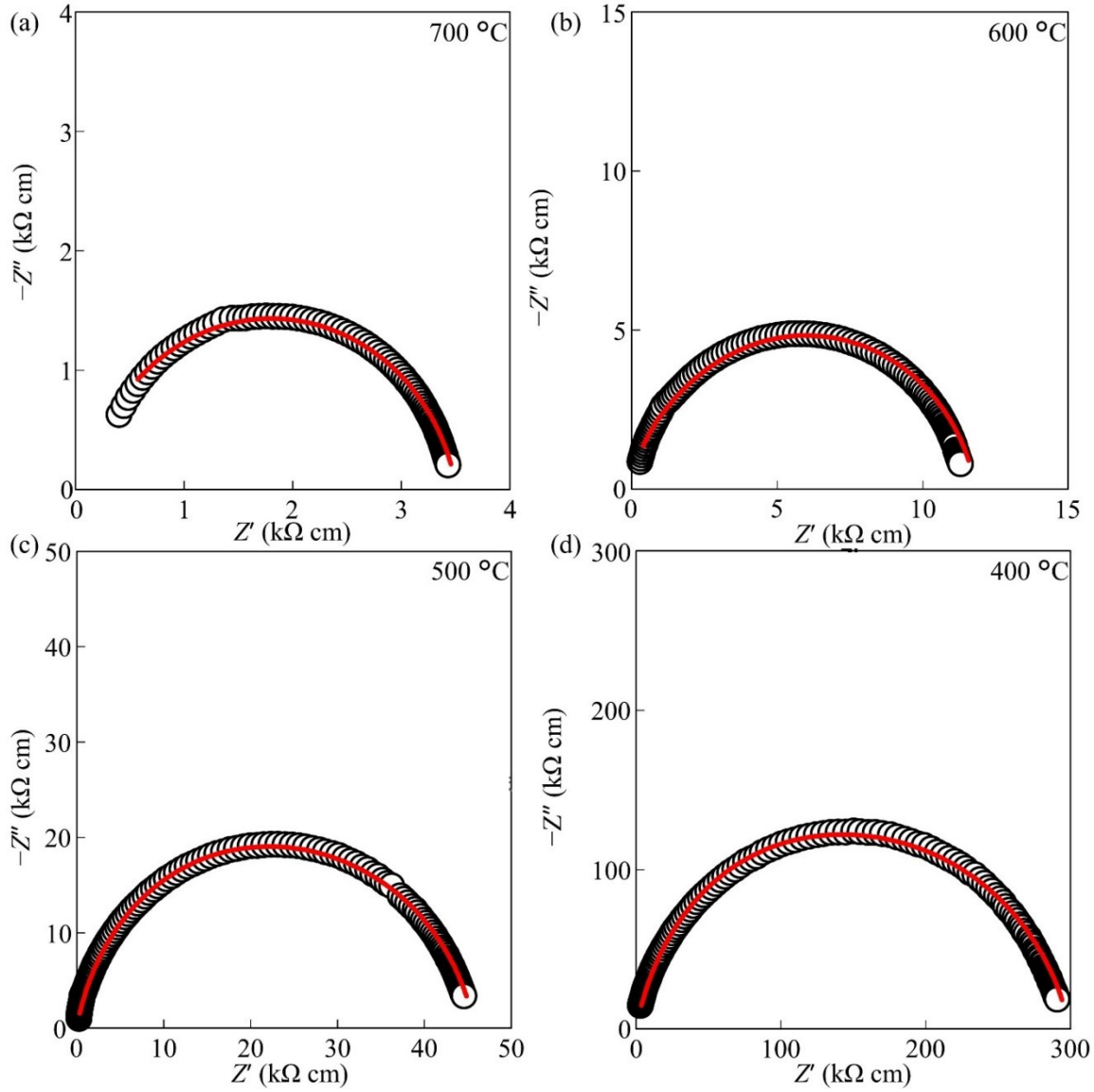

Fig. S9 Complex impedance plane plots of $BaGd_{0.9}Ca_{0.1}InO_{3.95}$ recorded in flowing N_2 gas at (a) 700 °C, (b) 600 °C, (c) 500 °C and (d) 400 °C. The red line and black circles denote the fit to the data and experimental data, respectively.

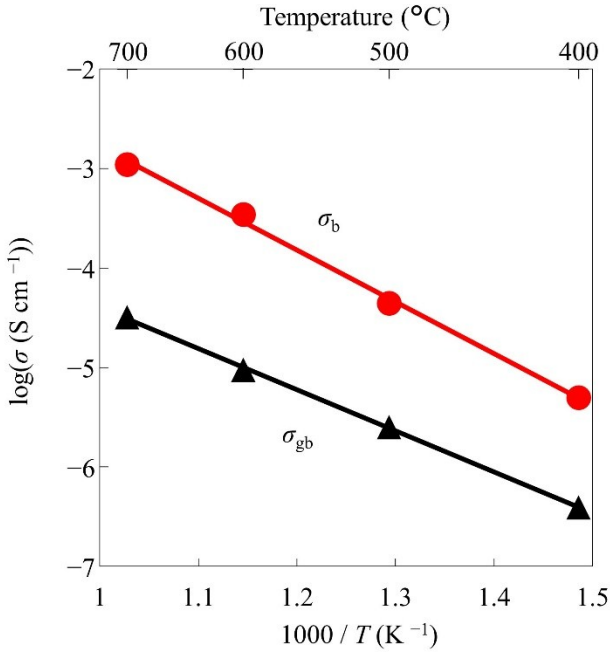

Fig. S10 Arrhenius plots of the bulk conductivity (red closed circles and red solid line, σ_b) and grain-boundary conductivity (black closed triangles and black solid line, σ_{gb}) of $BaGd_{0.9}Ca_{0.1}InO_{3.95}$ in flowing dry N_2 gas ($P(O_2) = 10^{-4}$ atm) in the electrolyte domain. The σ_b and σ_{gb} values were not corrected by the Bruggeman approximation. The activation energy for σ_b of $BaGd_{0.9}Ca_{0.1}InO_{3.95}$ was 1.03(4) eV.

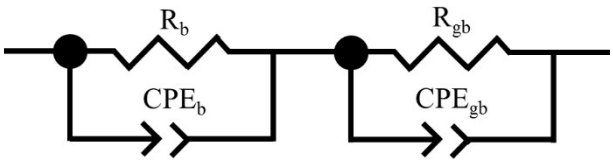

Fig. S11 Equivalent circuit used to fit the impedance spectroscopy data. *R* denotes a resistor and CPE stands for a constant phase element, the subscripts b and gb stand for bulk and grain boundary, respectively.

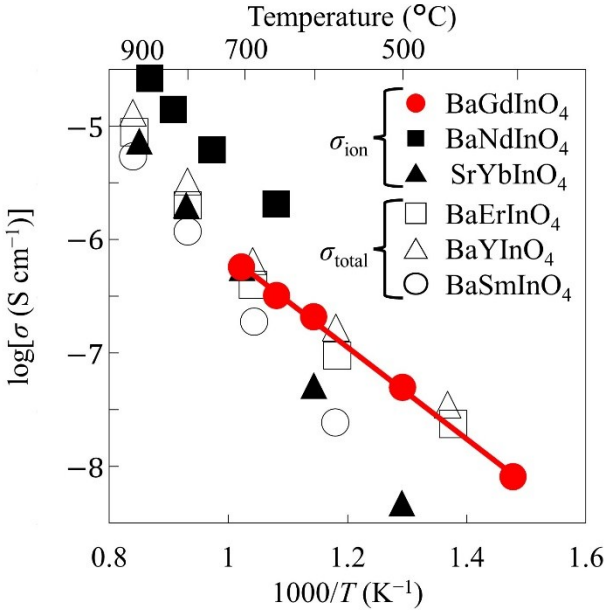

Fig. S12 Arrhenius plots of oxide-ion conductivities σ_{ion} of $BaGdInO_4$, $BaNdInO_4$ (Ref. 2) and $SrYbInO_4$ (Ref. 3) and total electrical conductivities σ_{total} of $BaErInO_4$, $BaYInO_4$ and $BaSmInO_4$ (Ref. 4). The σ_{ion} of $BaGdInO_4$ and $BaNdInO_4$ were measured in reduced atmospheres. The σ_{ion} of $SrYbInO_4$ and σ_{total} of $BaErInO_4$, $BaYInO_4$ and $BaSmInO_4$ were measured in static air. The σ_{ion} and σ_{total} values were not corrected by the Bruggeman approximation.

Single-crystal X-ray diffraction analysis of $BaGd_{0.9}Ca_{0.1}InO_{3.95}$

To determine the position of the Ca cation, twenty-one structure models (Model 1, Model 2, ···, Model 21) were investigated in preliminary structure refinements using SCXRD data (Table S6). The Model 19 where the Ca cation exists at Gd1 and Gd2 sites, g(Ca; Gd1) = 0.1, g(Gd; Gd1) = 0.9, g(Ca; Gd2) = 0.1 and g(Gd; Gd2) = 0.9, gave the best (lowest) reliability (R) factors in the SCXRD analyses. Here the $g(X; s)$ stands for the occupancy factor of X atom at the s site. Six structure models (Model A, Model B, ···, Model F) were also examined to investigate the positions of the oxygen vacancies in other preliminary structure refinements using the SCXRD data (Table S7). All the R factors for the six models almost equal. In the final refinement, we used the model F where all the occupancy factors equal to 0.9875.

Table S6 Results of the SCXRD analyses of $BaGd_{0.9}Ca_{0.1}InO_{3.95}$ based on the twenty-one structure models where the occupancy factors of cations are different from each other.[a]

			model									
	Site	Atom	1	2	3	4	5	6	7	8	9	10
Occupancy factors	Ba1	Ba	0.9	0.9	0.9	*0.8*	0.8	0.8	1	1	1	1
		Ca	0.1	0.1	0.1	0.2	0.2	0.2	0	0	0	0
	Ba2	Ba	0.9	0.9	0.9	1	1	1	0.8	0.8	0.8	1
		Ca	0.1	0.1	0.1	0	0	0	0.2	0.2	0.2	0
	Gd,Ca1	Gd	0.9	0.8	1	0.9	0.8	1	0.9	0.8	1	0.9
		Ba	0.1	0.2	0	0.1	0.2	0	0.1	0.2	0	0
		In	0	0	0	0	0	0	0	0	0	0.1
		Ca	0	0	0	0	0	0	0	0	0	0
	Gd,Ca2	Gd	0.9	1	0.8	0.9	1	0.8	0.9	1	0.8	0.9
		Ba	0.1	0	0.2	0.1	0	0.2	0.1	0	0.2	0
		In	0	0	0	0	0	0	0	0	0	0.1
		Ca	0	0	0	0	0	0	0	0	0	0
	In1	In	1	1	1	1	1	1	1	1	1	0.9
		Ca	0	0	0	0	0	0	0	0	0	0.1
	In2	In	1	1	1	1	1	1	1	1	1	0.9
		Ca	0	0	0	0	0	0	0	0	0	0.1
R factors		wR_2%	6.81	7.10	6.96	9.62	8.37	8.90	8.26	8.40	8.43	7.22
		R_1%(ob	2.84	2.88	2.86	3.47	3.32	3.34	3.27	3.32	3.30	2.88
		GoF	1.102	1.09	1.071	1.113	1.073	1.093	1.143	1.141	1.145	1.074

Table S6 (continued)

Table S6 (continued)

	Site	Atom	model 11	12	13	14	15	16	17	18	19	20	21
Occupancy factors	Ba1	Ba	1	1	1	1	1	1	1	1	1	1	1
		Ca	0	0	0	0	0	0	0	0	0	0	0
	Ba2	Ba	1	1	1	1	1	1	1	1	1	1	1
		Ca	0	0	0	0	0	0	0	0	0	0	0
	Gd,Ca1	Gd	0.8	1	0.9	0.8	1	0.9	0.8	1	0.9	0.8	1
		Ba	0	0	0	0	0	0	0	0	0	0	0
		In	0.2	0	0.1	0.2	0	0.1	0.2	0	0	0	0
		Ca	0	0	0	0	0	0	0	0	0.1	0.2	0
	Gd,Ca2	Gd	1	0.8	0.9	1	0.8	0.9	1	0.8	0.9	1	0.8
		Ba	0	0	0	0	0	0	0	0	0	0	0
		In	0	0.2	0.1	0	0.2	0.1	0	0.2	0	0	0
		Ca	0	0	0	0	0	0	0	0	0.1	0.1	0.2
	In1	In	0.9	0.9	0.8	0.8	0.8	1	1	1	1	1	1
		Ca	0.1	0.1	0.2	0.2	0.2	0	0	0	0	0	0
	In2	In	0.9	0.9	1	1	1	0.8	0.8	0.8	1	1	1
		Ca	0.1	0.1	0	0	0	0.2	0.2	0.2	0	0	0
R factors		wR_2%	7.59	7.63	8.56	8.63	8.99	8.24	8.55	8.57	4.98	8.10	9.58
		R_1%(ob	3.00	2.96	3.32	3.36	3.41	3.16	3.26	3.27	2.36	3.26	3.38
		GoF	1.074	1.070	1.092	1.114	1.085	1.081	1.087	1.088	1.087	1.101	1.077

Table S7 Results of the SCXRD analyses of $BaGd_{0.9}Ca_{0.1}InO_{3.95}$ based on the six structure models where the occupancy factors of oxygen atom are different from each other.

		Model A	B	C	D	E	F
Occupancy factors	O1	0.95	1	1	1	1	0.9875
	O2	1	0.95	1	1	1	0.9875
	O3	1	1	0.95	1	1	0.9875
	O4	1	1	1	0.95	1	0.9875
	O5	1	1	1	1	0.95	0.9875
R factors	wR_2%	5.04	5.00	5.00	5.02	5.00	4.98
	R_1%	2.37	2.37	2.38	2.37	2.37	2.37
	GoF	1.045	1.034	1.026	1.027	1.031	1.026

Table S8 Refined anisotropic atomic displacement parameters obtained by structure analyses of single-crystal X-ray diffraction data of $BaGd_{0.9}Ca_{0.1}InO_{3.95}$.

Site	U_{11} (Å^2)	U_{22} (Å^2)	U_{33} (Å^2)	U_{12} (Å^2)	U_{13} (Å^2)	U_{23} (Å^3)
Ba1	0.0104(2)	0.0114(2)	0.0130(2)	0	0.00192(18)	0
Ba2	0.0211(3)	0.0118(3)	0.0132(2)	0	−0.0010(2)	0
Gd,Ca1	0.00612(17)	0.00524(19)	0.00583(18)	0	0.00070(14)	0
Gd,Ca2	0.00714(17)	0.00452(18)	0.00472(18)	0	−0.00012(15)	0
In1	0.0054(2)	0.0058(3)	0.0053(2)	0	−0.00048(19)	0
In2	0.0068(2)	0.0059(3)	0.0060(2)	0	0.00055(19)	0
O1	0.014(3)	0.013(3)	0.005(3)	0	0.001(2)	0
O2	0.009(3)	0.032(4)	0.009(3)	0	−0.006 (2)	0
O3	0.0096(19)	0.014(2)	0.016(2)	0.008 (2)	−0.0040(18)	0.0020(16)
O4	0.015(2)	0.011(2)	0.0065(19)	0.0010(17)	0.0018(17)	−0.0009(17)
O5	0.015(2)	0.013(2)	0.009 (2)	−0.0006(17)	0.0021(18)	0.0061(17)

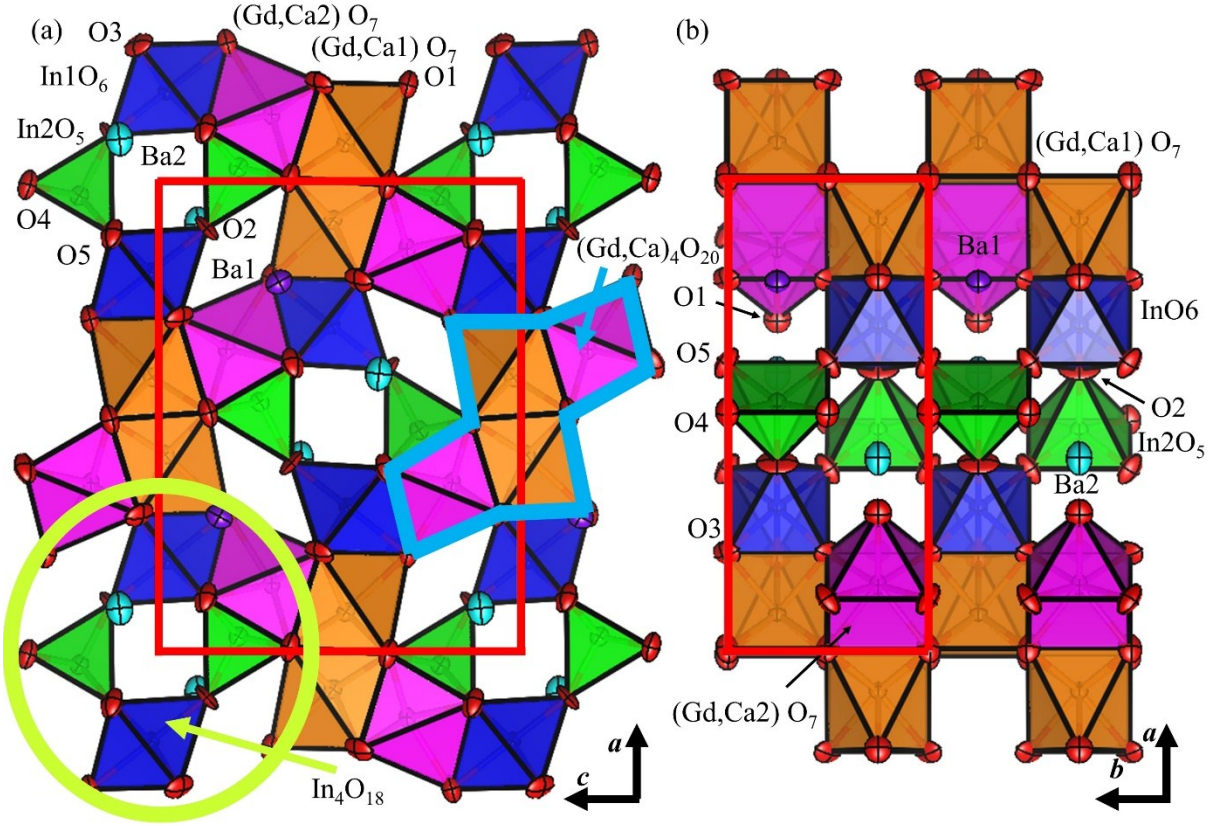

Fig. S13 Refined crystal structure of $BaGd_{0.9}Ca_{0.1}InO_{3.9}$ viewed (a) along the *b* axis ($-0.2 \le x \le 1.2$; $0.0 \le y \le 1.0$; $-0.25 \le z \le 1.25$) and (b) along the *c* axis ($-0.1 \le x \le 1.1$; $0.0 \le y \le 2.0$; $0.25 \le z \le 0.75$). The red solid lines represent the unit cell. Red, purple and light blue ellipsoids denote the oxygen, Ba1 and Ba2 atoms, respectively, where *Xn* denotes the *X* atom at the *Xn* site listed in Table 2. Blue, green, orange and pink polyhedra stand for $In1O_6$ octahedron, $In2O_5$ square pyramid, $(Gd,Ca1)O_7$ and $(Gd,Ca2)O_7$, respectively. Thermal ellipsoids are drawn at the 99% probability level. Yellowish green circle denotes In_4O_{18} four-membered ring. Light blue lines stand for a $(Gd_{0.9}Ca_{0.1})_4O_{20}$ unit.

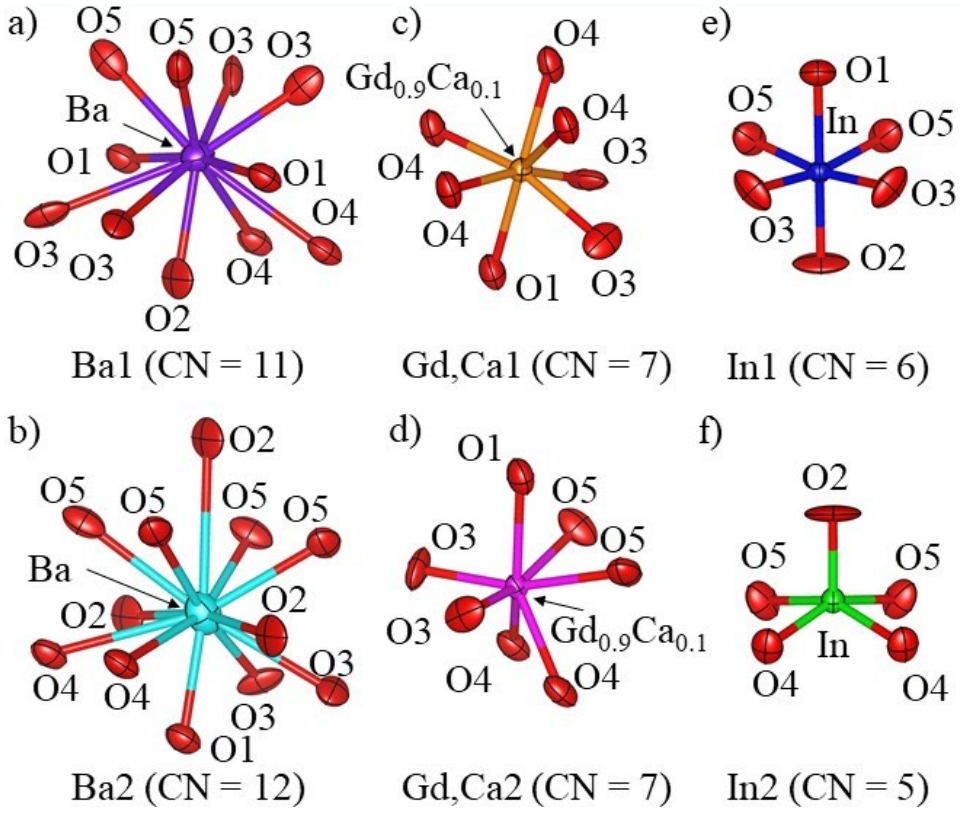

Fig. S14 Coordination environments of (a) Ba1, (b) Ba2, (c) Gd,Ca1, (d) Gd,Ca2, (e) In1 and (f) In2 cations. Red, purple, light blue, orange, pink, blue and green ellipsoids stand for oxygen, Ba1, Ba2, Gd,Ca1, Gd,Ca2, In1 and In2 atoms, respectively, where *Xn* denotes the *X* atom at the *Xn* site listed in Table 2. Thermal ellipsoids are drawn at the 99% probability level.

Crystal structure and bond valence-based energy (BVE) landscapes of $BaGdInO_4$, $BaNdInO_4$ and $SrYbInO_4$

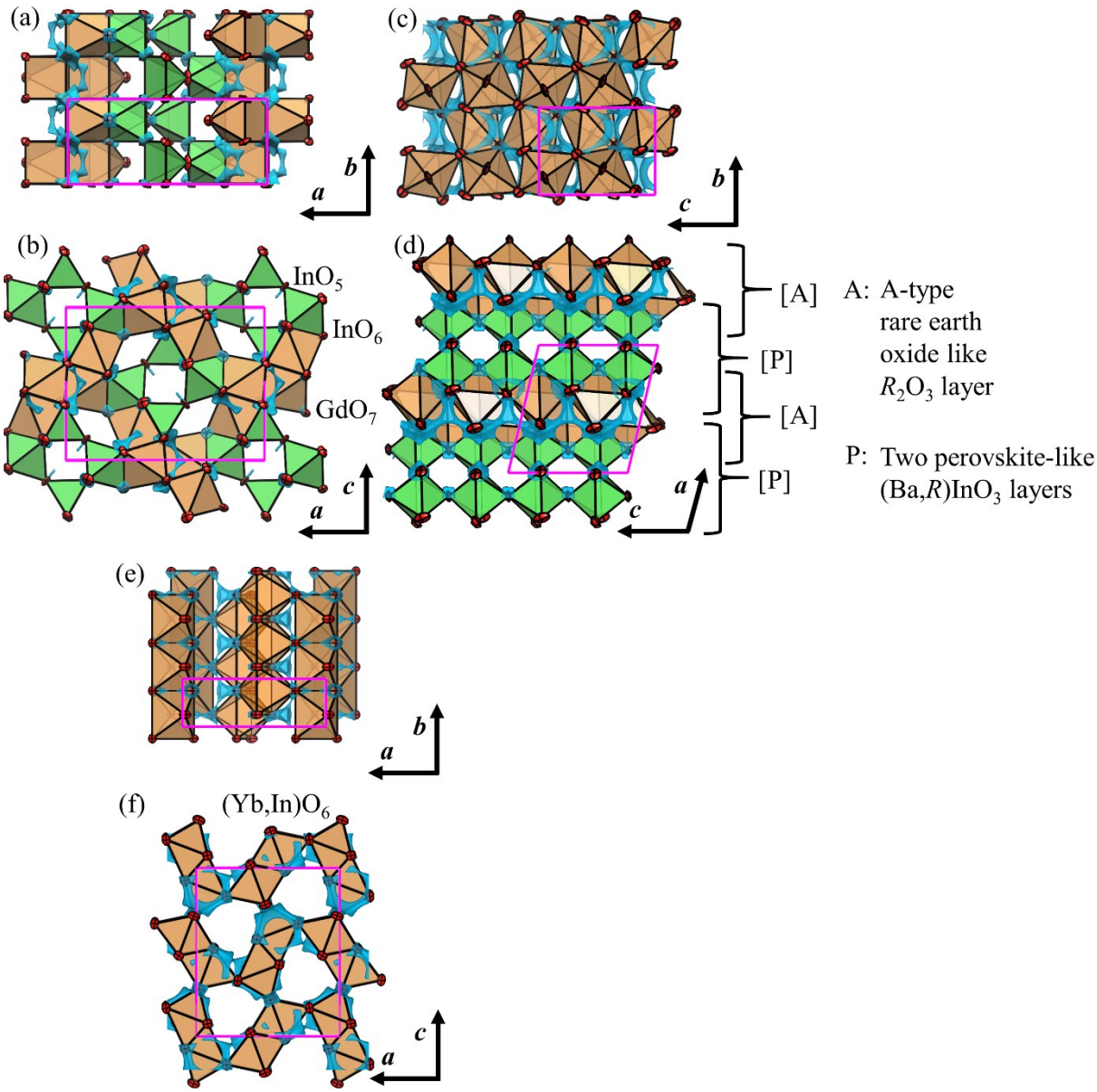

Fig S15 Bond valence-based energy (BVE) landscapes for an oxide ion with blue isosurfaces at 0.53 eV and crystal structure of $BaGdInO_4$ viewed (a) along the *c* axis ($-0.1 \le x \le 1.1$; $0.0 \le y \le 2.0$; $0.25 \le z \le 0.75$) and (b) along the *b* axis ($-0.2 \le x \le 1.2$; $0.0 \le y \le 1.0$; $-0.25 \le z \le 1.25$) where the crystallographic data obtained by the present SCXRD analysis were used. Red ellipsoids, green and orange polyhedra stand for oxygen atoms, InO_n (n = 5 and 6) and GdO_7, respectively. BVE landscapes for an oxide ion with blue isosurfaces at 1.31 eV and crystal structure of $BaNdInO_4$ (= $BaRInO_4$; R = Nd) viewed (c) along the *a* axis ($0.3 \le x \le 0.6$; $0.0 \le y \le 2.0$; $0.0 \le z \le 2.0$) and (d) along the *b* axis ($-0.2 \le x \le 1.6$; $0.0 \le y \le 1.0$; $0.0 \le z \le 2.0$) where the crystallographic data in Ref. 2 was used. Red ellipsoids, green and orange polyhedra stand for oxygen atoms, InO_6 and NdO_7, respectively. BVE landscapes for an oxide ion with blue isosurfaces at 0.58 eV and crystal structure of $SrYbInO_4$ (e) along the *c* axis ($-0.2 \le x \le 1.2$; $0.0 \le y \le 3.2$; $-0.2 \le z \le 0.2$) and (f) along the *b* axis ($-0.2 \le x \le 1.2$; $0.0 \le y \le 1.0$; $-0.2 \le z \le 1.2$) where the crystallographic data in Ref. 3 was used. Red ellipsoid and orange polyhedron stand for oxygen atoms and $(Yb,In)O_6$, respectively. Thermal ellipsoids are drawn at the 99% probability level. Pink solid lines denote the unit cells. Ba and Sr atoms are omitted in panels a-d and e,f, respectively, for simplicity.

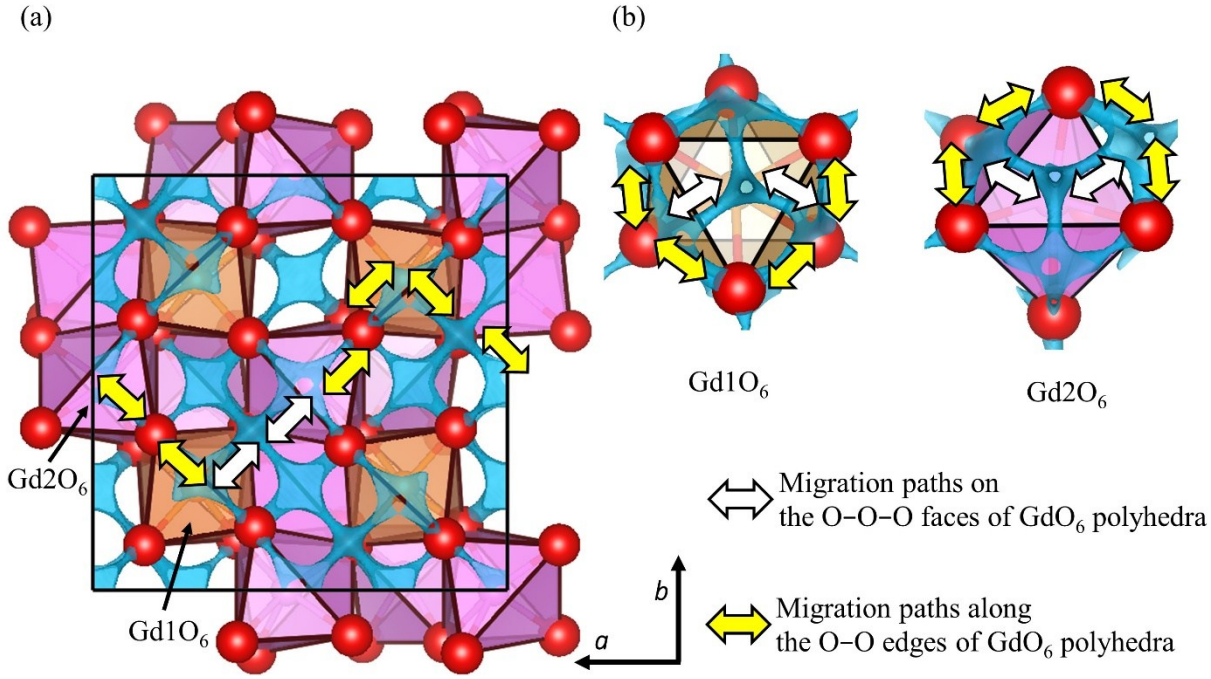

Fig. S16 (a) Bond-valence-based energy (BVE) landscape for an oxide ion with blue isosurfaces at 0.46 eV and crystal structure of Gd_2O_3 projected on the *ab* plane ($0.0 \le x \le 1.0$, $0.0 \le y \le 1.0$, $0.0 \le z \le 0.45$).
BVE landscapes for an oxide ion with blue isosurfaces at 0.46 eV around a $Gd1O_6$ polyhedron (b) and a $Gd2O_6$ polyhedron (c). Red, orange and pink spheres stand for oxygen, Gd1, Gd2 atoms, respectively. Orange and pink polyhedra stand for $Gd1O_7$ and $Gd2O_7$ polyhedra, respectively. Lattice parameter of Gd_2O_3 was a = 10.824(7) Å (Ref. 5). Atomic coordinates of Gd1, Gd2, O atoms are (0.25, 0.25, 0.25), (−0.032430, 0, 0.25) and (0.391, 0.1518, 0.3755), respectively.[5] Black solid lines denote the unit cells.

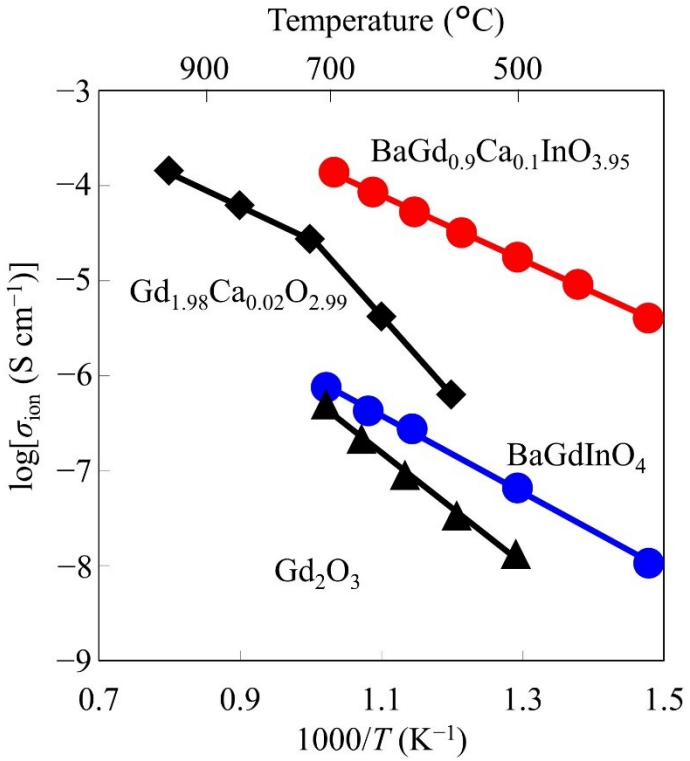

Fig. S17 Arrhenius plots of oxide-ion conductivities σ_{ion} of $BaGd_{0.9}Ca_{0.1}InO_{3.95}$, $BaGdInO_4$, $Gd_{1.98}Ca_{0.02}O_{2.99}$ (Ref. 6) and Gd_2O_3. Fig. S18 shown the σ_{total} of Gd_2O_3 was constant independent of $P(O_2)$. Therefore, it was suggested that the oxide-ion conduction is dominant in the electrolyte domains of the $P(O_2)$ range from 0.02 to 4×10^{-23} atm at 502 °C. The σ_{ion} values of $BaGdInO_4$, $BaGd_{0.9}Ca_{0.1}InO_{3.95}$, $Gd_{1.98}Ca_{0.02}O_{2.99}$ and Gd_2O_3 were corrected by the Bruggeman approximation.

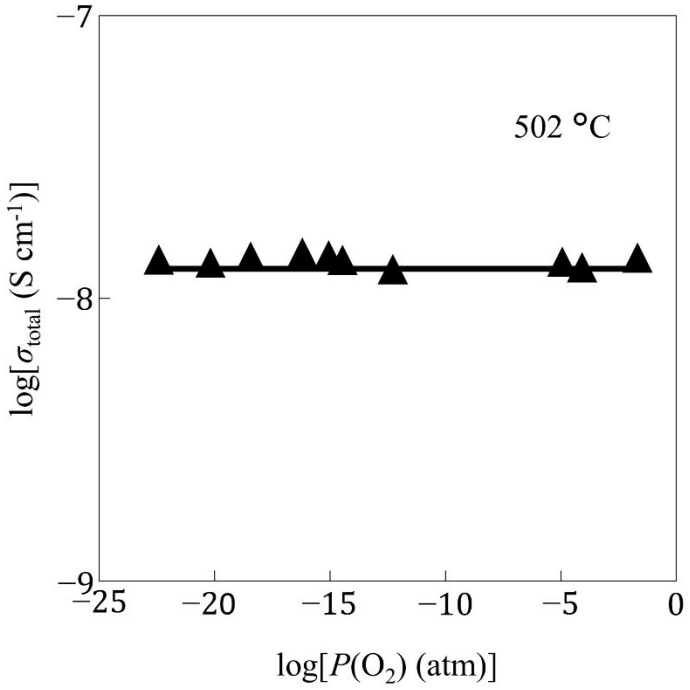

Fig. S18 Partial oxygen pressure $P(O_2)$ dependence of the total electrical conductivity σ_{total} of Gd_2O_3 at 502 °C. It is strongly suggested that the dominant carrier is oxide ion in the whole $P(O_2)$ region. The σ_{total} values were corrected by the Bruggeman approximation.

References

1 R. D. Shannon, *Acta Crystallogr. A*, 1976, **32**, 751–767.
2 K. Fujii, M. Shiraiwa, Y. Esaki, M. Yashima, S. J. Kim and S. Lee, *J. Mater. Chem. A*, 2015, **3**, 11985–11990.
3 A. Fujimoto, M. Yashima, K. Fujii and J. R. Hester, *J. Phys. Chem. C*, 2017, **121**, 21272–21280.
4 K. Fujii and M. Yashima, *J. Ceram. Soc. Japan*, 2018, **126**, 852–859.
5 I. P. Machado, V. C. Teixeira, C. C. S. Pedroso, H. F. Brito and L. C. V. Rodrigues, *J. Alloys Compd.*, 2019, **777**, 638–645.
6 T. Norby, O. Dyrlie, and P. Kofstad, *J. Am. Ceram. Soc.*, 1992, **75**, 1176–81.

End of ESI